CHEMISTRY
A EUROPEAN JOURNAL

DOI: 10.1002/chem.200601796

Structure of Ag Clusters Grown on F_s-Defect Sites of an MgO(100) Surface

Giovanni Barcaro,[a] Edoardo Aprà,[b] and Alessandro Fortunelli*[a]

Abstract: The structure of Ag_N clusters ($N=1$–4, 6, 8, 10), both in the gas phase and grown on the MgO(100) surface containing F_s-defects, has been investigated by a density functional basin-hopping (DF-BH) approach. In analogy with what observed in the case of gold clusters, it is found that the presence of the defect implies a double frustration and a cylindrical invariance of the metal–surface interaction, causing small Ag clusters growing around the F_s defect to be highly fluxional. Nevertheless, two different structural crossovers are found to be induced by the metal–defect interaction for the adsorbed clusters such that: 1) planar structures prevail for $N \leq 4$ (as in the gas phase); 2) noncrystalline (fivefold symmetric) structures, which are the lowest energy ones in the gas phase for medium sized Ag_N clusters ($N \geq 7$), prevail for $N=6$ and $N=8$; 3) distorted face-centered cubic (fcc) structures grown pseudomorphically on the defected surface prevail for $N=10$. The transition from fivefold to fcc motifs is rationalized in terms of the double-frustration effect, which increases the bond strain of the noncrystalline structures. Detrapping energies from the defect were also calculated; the lowest energy pathway corresponds to the detachment of a dimer.

Keywords: adsorption · cluster compounds · density functional calculations · silver · structure elucidation · surface chemistry

Introduction

Metal-on-oxide systems have attracted increasing attention in recent years in both science and technology for their interesting properties and their applications in the fields of catalysis, opto–electronic devices, chemical sensors, and so forth.[1–14] The knowledge of the cluster structure is an evident pre-requisite for a deep understanding of these fascinating properties, and much theoretical effort has been devoted to this subject, primarily focusing on small clusters, especially when high accuracy was pursued through the use of sophisticated, first-principle approaches. In this context, the MgO(100) surface has often been studied for various reasons, ranging from its widespread use as an inert support, to the simplicity of its theoretical description.[15–18] MgO(100) is in fact an apolar, simple ionic surface without the complications associated with surface reconstruction, and so forth.[2,19,20] After initial studies of the interaction of metal atoms with the regular surface,[15,16,21,22] it was soon realized that the presence of kinks, corners, local defects, such as the oxygen vacancy (also called F_s or color center due to its optical absorption properties), and so forth, could substantially modify the metal–oxide interaction.[7,16,18,23–26,28–30,55] This assumes particular importance in the study of the growth process. Especially for metals such as silver, which presents a very weak adhesion to the regular surface ,[31] and hence diffuses rapidly even at low temperatures,[15,18,32–34] the presence of defects acting as trapping centers is reputed necessary for nucleation to occur, even more than, for example, in the Pd/MgO(100) case.[35] In this perspective, an important issue thus concerns the influence of the metal/defected-surface (rather than regular-surface) interaction on the cluster structure, i.e., whether the metal clusters keep their gas-phase structure, or whether the interaction with the defected site is strong enough to induce structural transitions.[7,18,23–26,55] In the present article, we tackle this issue by studying the structure of small (up to ten atoms) silver clusters both in the gas phase and adsorbed on the F_s-defective MgO(100) surface. The F_s defect on the MgO(100) surface is chosen as a prototypical example of a neutral local defect. We focus on clusters in the size range $N=1$–10 ($N=$number of Ag atoms), which are small enough to be computationally affordable and appreciably influenced by the presence of the local de-

[a] Dr. G. Barcaro, Dr. A. Fortunelli
Molecular Modeling Laboratory, IPCF-CNR
Via G. Moruzzi 1, Pisa, 56124 (Italy)
Fax: (+39) 050-3152442
E-mail: fortunelli@ipcf.cnr.it

[b] Dr. E. Aprà
Computer Science and Mathematics Division
Oak Ridge National Laboratory
Oak Ridge, TN 37831 (USA)

fects at the cluster–surface interface, but large enough to allow identification of structural motifs and to study their energetic crossover. We use a systematic search protocol within a first-principles approach: a density-functional basin-hopping (DF-BH) algorithm,[36] which is CPU-intensive, but gives us some confidence of having singled out the global minimum and the lowest energy excited states at each size. We find that indeed the presence of the defect substantially alters the potential-energy landscape of adsorbed Ag clusters, favoring (distorted) face centered cubic (fcc) structures with respect to noncrystalline fivefold symmetric configurations, which are the ground state for gas-phase Ag clusters of size $N \geq 7$.

The article is arranged as follows. After a brief review of previous work, the computational approach is described (Computation Methods). The results of the DF-BH calculations for both gas-phase and adsorbed clusters are presented, and distinguished in terms of the cluster size (Results and Discussion). Conclusions are summarized.

Previous work: Concerning previous work on the Ag and MgO(100) systems, a wealth of experimental and theoretical information exists on gas-phase Ag clusters. Extensive references to small ($N < 6$) clusters can be found in reference [37], while for larger clusters the main contributions are references [37–40], in which the structure of Ag clusters (and their ions) up to 12–13 atoms have been systematically investigated. Our calculations are in qualitative (and often quantitative) agreement with former DF calculations,[37,40] but a detailed comparison is not presented, as it would not be very informative.

The F_s center is one of the most studied defects of the MgO(100) surface.[16,27–30,41–60] Both static and dynamic properties have been studied: electron density maps and density of states plots,[29,46] formation energy and diffusion energy barriers,[27,41–44] and optical properties.[28,30] Intense study has also been conducted on metal clusters adsorbed on the F_s defect.[16,30,48–60] Despite recent suggestions that this type of defect might not be abundant on carefully annealed MgO(100) films,[61–65] it can be easily created by electron bombardment or other means[30,63] and it has been suggested that it can have an important effect on the catalytic activity of extremely small supported clusters.[58,63]

Computational Methods

The search for the lowest energy structures of Ag clusters was performed either by a biased search starting from selected configurations or by a density-functional basin-hopping (DF-BH) approach.[36] The basin-hopping algorithm[66–68] is defined in the following steps: 1) an initial random configuration was chosen, a local geometry optimization was performed, and the final energy (the fitness parameter) was registered as E_1; 2) starting from the relaxed configuration, the atoms of the metal cluster were randomly displaced,[69] a new local geometry optimization was performed, and the final energy is registered as E_2; 3) a random number (rndm) between 0 and 1 was generated and the movement of step 2 was accepted only if $\exp[-(E_2-E_1)/k_BT] > \text{rndm}$ (Metropolis criterion); 4) steps 2 and 3—the Monte Carlo steps—were repeated a given number of times. Depending on the k_BT parameter (which in this work is set to 1.0 eV in all the calculations), some high-energy configurations were accepted and the search was able to explore different structural motifs (belonging to different funnels of the potential-energy surface) of the metal cluster. In the DF-BH approach,[36] the determination of energies and forces was achieved by using a first-principles DF method: the number of Monte Carlo steps was limited by the CPU time available, and the DF-BH approach is practically unfeasible in the case of systems composed by more than few tens of atoms. In the present case, we deal with metal clusters composed of up to ten atoms, and we expected the global minimum for each cluster to be located in a small number of Monte Carlo steps.

The DF-BH calculations were carried out by employing a cluster approach[70] for the description of the MgO support. Either an ($Mg_{18}O_{18}$) cluster of C_{2v} symmetry or an ($Mg_{25}O_{25}$) cluster of C_{4v} symmetry (see Figure 1) were chosen, depending on the size of the metal aggregate.

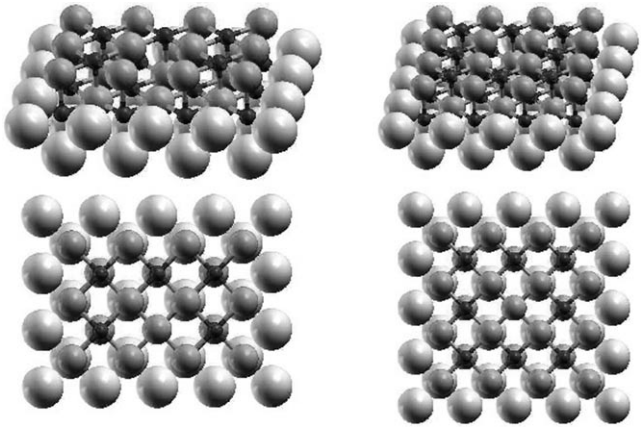

Figure 1. The systems used to model the F_s-defective MgO(100) surface in the cluster approach; small atoms represent oxygen atoms, larger atoms magnesium atoms, and largest atoms the positive charge sites on which a repulsive pseudopotential is added.

Both MgO clusters were embedded in an array of ± 2.0 au point charges[71] (about 1500) extending for four layers in the direction perpendicular to the surface and up to ≈ 10 Å from the borders of the cluster in the (100) surface plane. The atoms of the central cluster and the point charges around it were located at the lattice positions of the MgO rock-salt bulk structure at the experimental lattice constant of 4.208 Å. Moreover, a repulsive pseudopotential[72] was added on the positive point charges in direct contact with the cluster, in order to avoid an unphysical polarization of the charge density.[73] As shown in Figure 1, to create an F_s vacancy we erased a neutral oxygen atom from the surface keeping frozen the coordinates of all the Mg and O atoms around the defect. Structural relaxation around the F_s defect has been show to be undramatic[19,41,74,75] and we did not expect that the modest interaction of Ag clusters[76] with the surface would qualitatively modify the results (this has been actually been checked in selected cases). Moreover, freezing the geometry of the oxide substrate at its experimental equilibrium configuration was, in our opinion,[77] the best choice not to let the DF/GGA approach overestimate the structural relaxation around the oxygen vacancy upon metal adsorption. All the calculations with the cluster approach were carried out with the DF module of the NWChem package[78] by using the PW91 xc-functional[79] in the spin-unrestricted formalism. The geometry optimizations were performed by using Gaussian-type orbital basis sets of double-ζ quality,[80] while the total binding energy used in the Metropolis criterion energy was calculated from a single-point calculation on the relaxed geometry by using a triple-ζ plus polarization basis set.[80] A 19-valence-electron effective core potential was used for Ag.[81] The two electrons trapped in the cavity were described with a Gaussian-type orbital basis set of double-ζ quality for the optimization run and a set of triple-ζ quali-

ty plus d polarization functions in the single-point final calculation.[82] Charge-density-fitting Gaussian-type orbital basis sets were used to compute the Coulomb potential.[83] The calculations used a Gaussian-smearing technique[84] (with a smearing parameter of 0.001 a.u.) for the fractional occupation of the one-electron energy levels.

After having singled out the low-energy structures at each size by using the DF-BH approach with the NWChem software and a cluster description of the oxide, the obtained results were validated by performing local geometry optimizations with the PWscf (plane-wave self-consistent field) computational code,[85] employing the PBE xc-functional[86] and ultrasoft pseudopotentials in the spin-unrestricted formalism. This approach was computationally more demanding, but was essentially free of basis set limitations and thus represents a good check of localized basis set calculations. The kinetic energy cutoff for the selection of the plane-wave basis set was fixed at 20 au for all the calculations. A (3,3,1) *k*-point sampling of the Brillouin zone was chosen, and a Gaussian smearing technique (with a smearing parameter of 0.001 au) was applied. The MgO(100) surface was modeled by a three-layer slab, each layer containing 18 (3×3 cell) or 24 (4×3 cell) Mg and O atoms fixed in the lattice positions of the rock-salt bulk structure. The unit cell was chosen such that the distance between metal clusters belonging to replicated cells was greater than 6–8 Å. The F_s defect was created by removing a neutral oxygen atom from the surface and freezing the coordinates of all the other atoms of the substrate in the lattice positions.

It is important to stress that the two approaches: the cluster approach using NWChem and the periodic cell approach using PWscf, produced the same qualitative results with minor quantitative differences (partly due to the slightly different xc functionals adopted in the two cases). The energy values reported in the following are those obtained using the PWscf code.

Results and Discussion

In this section we report and discuss the results regarding the low-energy structures for Ag_N clusters (with $N=1$–4, 6, 8, 10) both in the gas phase and adsorbed on the F_s defect of the MgO(100) surface.

It is convenient to define four quantities: 1) the adhesion energy (E_{adh}), calculated by subtracting the energy of the oxide surface and of the metal cluster, both frozen in their interacting configuration, from the value of the total energy of the system, and by taking the absolute value; 2) the binding energy of the metal cluster (E_{met}), calculated by subtracting the energy of the isolated metal atoms from the total energy of the metal cluster in its interacting configuration, and by taking the absolute value; 3) the metal cluster distortion energy (E_{dist}), which corresponds to the difference between the energy of the metal cluster in the configuration interacting with the surface minus the energy of the cluster in its lowest energy gas-phase configuration (thus, a positive quantity); and 4) the total binding energy (E_{bnd}), which is the sum of the binding energy of the metal cluster and of the adhesion energy ($E_{bnd}=E_{adh}+E_{met}$).

In the following, the results are distinguished in terms of the Ag cluster size. For Ag_N with $N=2$–4, due to the small size of the metal clusters, we performed a biased DF search by locally optimizing a limited number of physically reasonable configurations, both in the gas phase and when adsorbed on the defected surface. The configurations of the adsorbed Ag_N clusters with $N=2$, 4 have been reported in previous work[49,50] with the exception of configuration (c1) of the tetramer (see below). The present results are in qualitative (and often quantitative) agreement with these earlier investigations, and are briefly reported in the following to set the stage for larger clusters and the sake of completeness. For Ag_6, three DF-BH runs were performed, each composed of 15 Monte Carlo steps; for Ag_8 and Ag_{10}, five DF-BH runs were performed, each composed of 15 Monte Carlo steps, both in the gas phase and when adsorbed on the defected surface. The starting configurations of each run were generated randomly in a sphere of radius 4 Å around the vacancy.

To our knowledge, this is the first time that a DF-BH approach has been applied to metal clusters adsorbed on a surface. The DF-BH approach is useful to sample the PES of these complicated systems in which biased searches often miss the ground-state structure for small clusters.

Single-atom adsorption topography: A single Ag atom interacts preferentially with the oxygen site of the regular (100) surface, with an adhesion energy of about 0.4 eV.[15,16,18,33,87] The presence of the F_s defect increases the interaction energy to 1.64 eV.[16,18,51] This increase can be rationalized in terms of two effects: first, the removal of an oxygen atom determines a remarkable reduction of the Pauli repulsion between the electronic cloud of the metal and that of the oxide substrate; second, the two electrons trapped in the cavity, being weakly bound by the Madelung potential, are very polarizable and able to form a stronger bond with the metal atom. The decrease of the Pauli repulsion determines also a reduction of the equilibrium distance of the metal atom from the surface (from a value of ≈2.5 Å on the oxygen site of the regular surface, to a value of ≈2.0 Å on top of the defect). The presence of the F_s defect not only modifies the adsorption on top of it,[16,18,51] but also the whole adhesion topography in an area which extends up to distances of 4–6 Å from the vacancy.[26,74,77] For example, the adhesion of the Ag atom on top of an Mg-atom nearest neighbor of the vacancy is 0.78 eV, much bigger than the value 0.22 eV characterizing the same site on the regular surface. In Figure 2, the topographic landscapes of the metal–surface interaction in the case of adsorption of a single Ag atom are displayed; for comparison, the topographic landscapes for the regular surface are also shown. The profiles in Figure 2 were obtained by performing a vertical relaxation of the Ag atom on top of several sites of the MgO regular and defective unit cell and interpolating the points obtained; in Figure 2a and 2c the adhesion energy and in Figure 2b and 2d the equilibrium distance from the surface are shown for the regular and defective surfaces, respectively. These profiles are qualitatively similar to those reported in reference [77] for the adsorption of a gold atom. As shown in Figure 2c, the presence of the defect produces a large basin of attraction, exhibiting an approximate cylindrical symmetry around the vacancy. Furthermore, on top of the defect the increase of the adhesion energy corresponds to a decrease of the equilibrium distance, whereas on the neighboring sites the increase of the adhesion often corre-

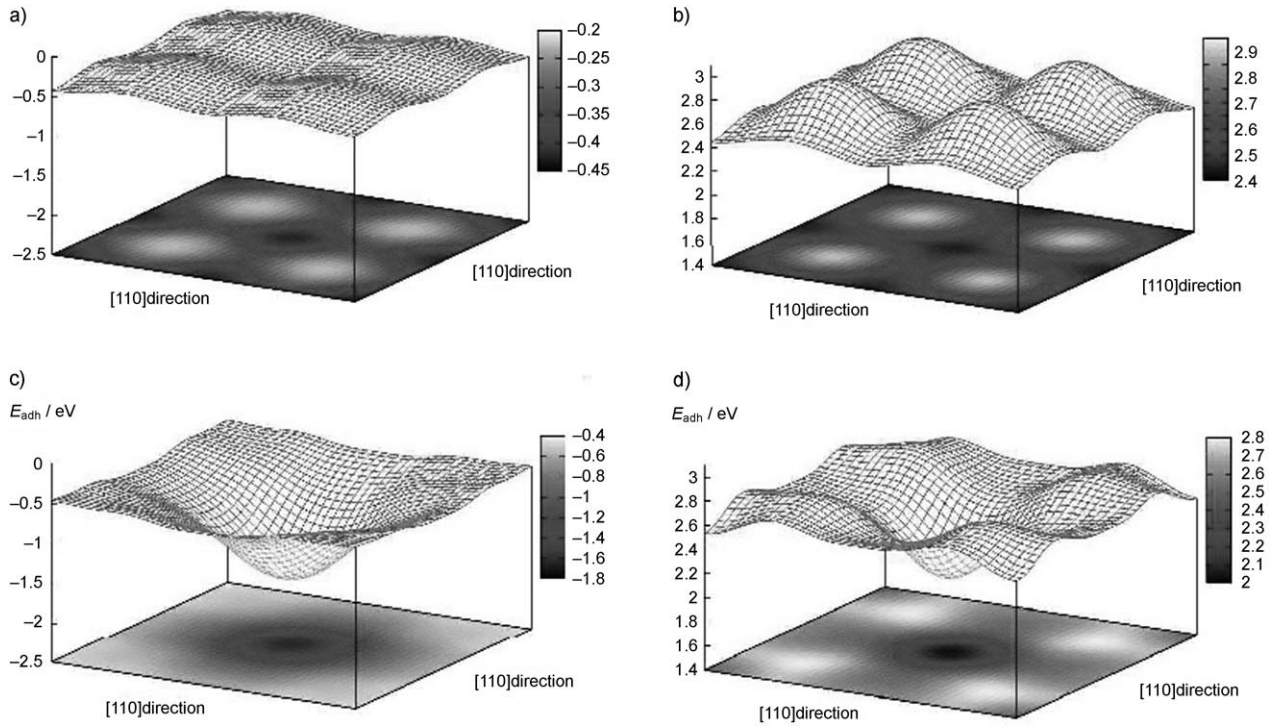

Figure 2. Topographic landscape of the adsorption of an Ag atom on the MgO(100) surface: the adhesion energy (a,c) and the equilibrium distance from the surface (b,d) are shown for the regular surface and the F_s-defective surface, respectively.

sponds to a lengthening of the metal–surface equilibrium distance. As we will see in the following discussion, the approximate cylindrical symmetry around the defect is also present when small clusters are adsorbed on the defect and implies a *rotational invariance* by which small clusters can rotate almost freely around an axis perpendicular to the surface, keeping one atom firmly bound to the defect. Moreover, the strong variation of the equilibrium distance around the defect implies that metal cluster growth is frustrated not only horizontally with respect to the surface (due to the mismatch between the lattice constants of the metal and of the support), but also vertically because of the difference between the equilibrium distance on top of the defect and that on top of the neighboring site around the vacancy, an effect that we have called *double frustration*.[77]

Ag_2, Ag_3, and Ag_4 clusters: The configurations considered for Ag_N ($N=2$–4) clusters adsorbed on the F_s defect are displayed in Figure 3, while the corresponding energy analysis is reported in Table 1.

When a second Ag atom reaches the defect, it binds to the first one in such a way that the dimer axis results perpendicular to the surface, as shown in previous work.[18,49,55] This configuration is stabilized by the electrostatic contribution coming from the increased polarization of the metal electronic density of the dimer in the field of the oxide. In general, it has been noted[18,49,55,56,87] that the presence of metal atoms above those directly interacting with the surface increases the adhesion energy: this effect is what we have called "metal-on-top" stabilization mechanism.[18] Thanks to the metal-on-top effect, the adhesion energy of the dimer is 1.79 eV, increased with respect to the adhesion of the single atom on the defect, despite the fact that the atom interacting with the surface is involved in a strong

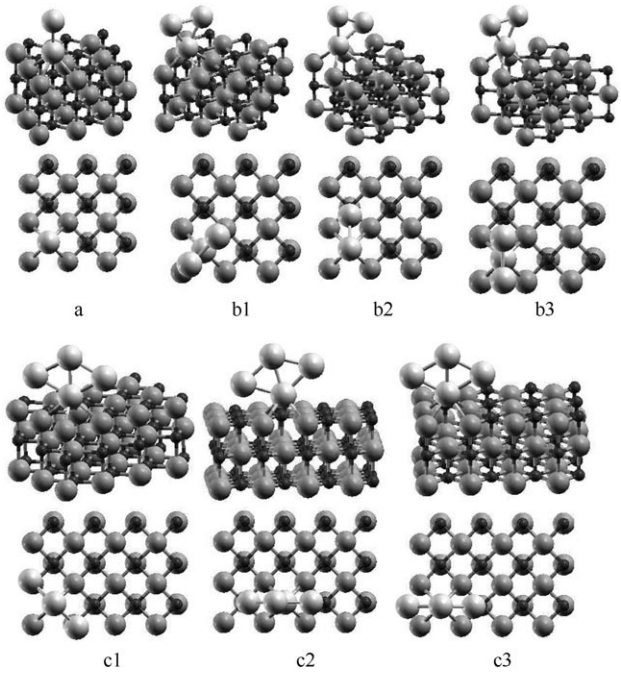

Figure 3. Schematic representation of the lowest energy structures and saddle points of Ag_N ($N=2$–4) clusters on the F_s-defective MgO(100) surface.

Table 1. The values of the various energy quantities defined in the text are reported for the lowest energy structures and saddle points of Ag_N ($N=1$–10) clusters. The notation used refers to the nomenclature defined in Figures 3–6. All energy values in eV.

Cluster	Conf.	E_{adh}	E_{met}	E_{dist}	E_{bnd}	Spin
Ag_1		1.64	–	–	1.64	1/2
Ag_2	a	1.79	1.72	0.01	3.51	0
Ag_3	b1	2.23	2.57	0.03	4.80	1/2
	b2	2.18	2.59	0.01	4.77	1/2
	b3	2.15	2.60	0.00	4.75	1/2
Ag_4	c1	2.46	4.55	0.02	7.01	0
	c2	2.48	4.52	0.05	7.00	0
	c3	2.43	4.55	0.02	6.98	0
Ag_6	d1	2.74	7.95	0.55	10.70	0
	d2	2.80	7.88	0.62	10.68	0
	d3	2.82	7.91	0.59	10.73	0
	d4	2.83	7.81	0.69	10.64	0
	d5	2.66	7.85	0.65	10.51	0
	d6	2.34	8.31	0.19	10.65	0
	d7	1.88	8.38	0.12	10.26	0
Ag_8	e1	2.02	12.29	0.06	14.31	0
	e2	2.19	12.09	0.25	14.28	0
	e3	2.14	12.13	0.22	14.27	0
	e4	2.03	11.99	0.35	14.02	0
	e5	2.07	12.21	0.14	14.28	0
	e6	2.30	11.53	0.82	13.83	0
Ag_{10}	f1	2.43	15.60	0.05	18.03	0
	f2	2.61	15.57	0.08	18.18	0
	f3	2.24	15.07	0.58	17.31	0
	f4	2.52	15.37	0.29	17.89	0
	f5	2.56	15.44	0.21	18.00	0
	f6	2.82	15.47	0.18	18.29	0

metallic bond, which should decrease its availability to interact with the surface.

The third atom is then added in a cluster plane perpendicular to the surface. When the cluster plane is oriented along the [100] direction, we obtain the ground-state configuration, exhibiting C_{2v} symmetry and labeled as b1. A 45° rotation brings the plane of the cluster along the [110] direction and the cluster slightly bends in order to make one of the two upper Ag atoms adhere to one oxygen ion of the surface nearest neighbor of the vacancy: this local minimum, labeled as b2, is higher in energy than the ground state by only 0.03 eV. The configuration b2 can be converted into another configuration b2 passing through the saddle point b3, in which the cluster is still oriented along the [110] direction with symmetry C_{2v} and which is higher in energy than the configuration b2 by 0.02 eV (thus is 0.05 eV higher than the ground state). The small energy differences between the three configurations confirm the rotational freedom of the metal cluster around an axis perpendicular to the surface and passing through the metal atom bound to the defect. The doublet spin state of the trimer is responsible for the fluxional character of the metal cluster and consequently for the small values of the metallic distortion energy for the three configurations.

The case of the tetramer is very similar to that of the trimer: Ag_4 adsorbs in a rhombic configuration (the same characterizing the gas phase at this size[88]) with one of the two highly coordinated vertices anchored to the vacancy and the cluster plane perpendicular to the surface. The ground-state configuration c1 corresponds to the cluster plane oriented along the [100] direction and has C_{2v} symmetry. Also in this case, a 45° rotation to the configuration c2 is accompanied by a bending of the cluster, so that one of the two lower coordinated vertices adheres to one oxygen ion of the surface nearest neighbor of the vacancy; this configuration has been previously found in reference [50]. The transition between two analogous configurations c2 is represented by the saddle point c3 with C_{2v} symmetry. As in the case of the trimer, the energy differences between the three configurations are very small (below 0.05 eV), thus confirming the rotational freedom of Ag_4.

Ag_6 cluster: The results concerning the Ag_6 cluster are reported in Table 1 and the corresponding structures are displayed in Figure 4. In the same figure, the three lowest energy configurations characterizing Ag_6 in the gas phase are also displayed.

The ground state of the cluster in the gas phase is represented by the planar structure a, with cohesive energy of

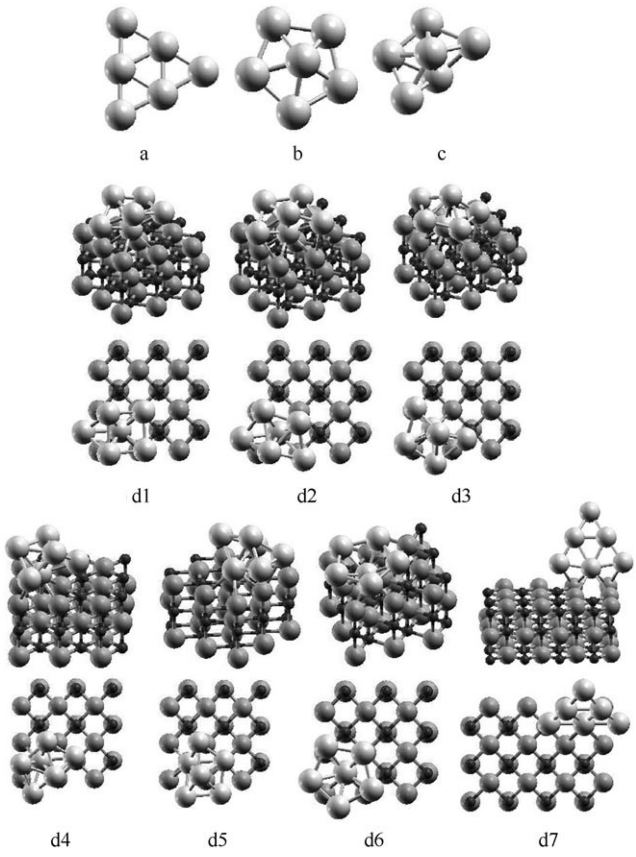

Figure 4. Schematic representation of the lowest energy structures of Ag_6 both in the gas phase (a–c) and on the F_s-defective MgO(100) surface (d1–d7).

8.50 eV; a pentagonal pyramid, structure b, has a cohesive energy a bit smaller than that of the ground state (8.30 eV), while structure c, an incomplete pentagonal bipyramid missing one equatorial atom, has a cohesive energy of 7.86 eV. These results are in keeping with the previous literature.[37,38,40] All three structures correspond to singlet spin states. At this size, the planar configuration has an enhanced stability as six is a magic number of the 2D triangular jellium model:[89] indeed, the HOMO–LUMO gap for this structure is 2.15 eV.

When Ag_6 adsorbs on the surface, we find three low-energy configurations, d2–d4, which belong to the same structural family, that is, the incomplete pentagonal bipyramid—the structure c of the gas phase. Among this family, configuration d3 is the ground state. The presence of the defect thus causes a first structural transition from a planar structure (favored in the gas phase) to noncrystalline (fivefold symmetric) structures (favored for adsorbed Ag_6). These three configurations can be obtained from each other through small rotations around an axis perpendicular to the surface and passing through the defect. From the energy values in Table 1, we can see that the small differences in the values of the total binding energies imply a rotational freedom of the metal cluster around the F_s vacancy.

In contrast, configurations d1 and d5 represent two local minima derived from a distortion of the motif of the incomplete bipyramid: they can be seen as two square pyramids with the square basis either on top to the atom directly bound to the defect (structure d1) or grown quasi-pseudomorphically on the defect and on three oxygen surface ions near the vacancy (structure d5). In both cases, the fifth atom is grown tetrahedrally on a triangular face of the pyramid. These two configurations have an increased metallic energy, but also a decreased adhesion to the surface. Configuration d1 turns out to be competitive with the global minimum, whereas structure d5 lies higher in energy by about 0.2 eV.

In structure d6 the metal cluster has the shape of a pentagonal pyramid (configuration b of the gas phase): in this motif the metallic bond results remarkably stabilized, but the adhesion to the surface is weaker. Thanks to compensation between these two contributions, this configuration is also competitive with the ground state.

Finally, in structure d7, the metal cluster is quasi-planar and adsorbed with three metal atoms interacting with the vacancy and two nearest-neighbor oxygen atoms (the cluster is slightly tilted with respect to the surface). This configuration is higher in energy by about 0.5 eV, despite the fact that this corresponds to the most stable structural motif characterizing the gas phase. This fact can be rationalized by considering the shape of the topography around the defect, which suggests a better adhesion for structure belonging to compact motifs, such as the pentagonal pyramid or the incomplete pentagonal bipyramid. The gain in adhesion is able to compensate for the loss of metallic energy in these motifs.

It can be noted that we discuss not only the putative global minimum, but also the putative lowest energy isomers. In principle, the DF-BH is also able to single out these higher energy configurations, even though longer and more numerous Monte Carlo runs would be necessary in order to ensure that the first, for example, three or four isomers have been correctly located, and assured that the intermediate configurations in the structural interconversion are not much higher in energy than the k_BT parameter. Due to the small size of the clusters here investigated, we are confident that most important structural motifs of these clusters are depicted in Figures 4–6.

We conclude that at this size the competition between metal bonding and adhesion, together with phenomena such as rotational invariance and double frustration, determine the presence of structures belonging to different structural motifs but exhibiting very similar values of the total binding energy: this implies a fluxionality of the metal cluster adsorbed on the defected surface. Nevertheless, a structural transition from planar to fivefold structures induced by the metal–defect interaction is clearly observed.

Ag_8 cluster: The results concerning Ag_8 are reported in Table 1 and the corresponding structures are displayed in Figure 5. In the same figure, four low-energy configurations

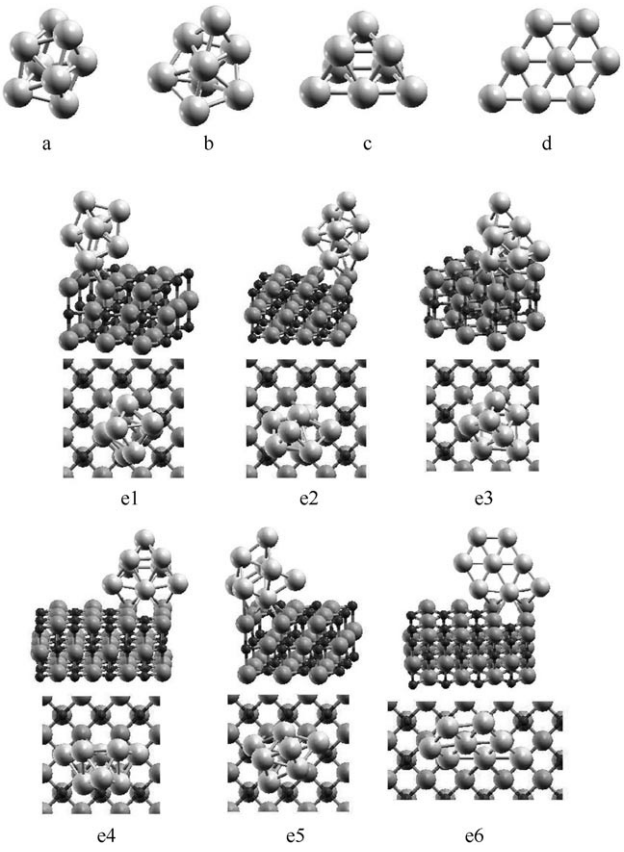

Figure 5. Schematic representation of the lowest energy structures of Ag_8 both in the gas phase (a–d) and on the F_s-defective MgO(100) surface (e1–e6).

characterizing Ag_8 in the gas phase are also displayed, which are in keeping with previous literature.[37,38,40] In the gas phase the ground-state, structure a, is represented by a pentagonal bipyramid in which one equatorial atom has been substituted by a dimer with the axis perpendicular to the equatorial plane (cohesive energy of 12.35 eV). Structure b belongs to the same structural motif, except that, in this case, the pentagonal bipyramid is perfect and the eighth atom is grown tetrahedrally on one of the ten triangular facets (cohesive energy of 12.21 eV). Structure c, almost isoenergetic with b, belongs to a crystalline motif: it is formed by a central octahedron with two atoms grown tetrahedrally on two opposite facets of the same square pyramid (cohesive energy of 12.19 eV). The planar structure d results destabilized with respect to the ground state and has a cohesive energy of 11.67 eV. For gas-phase Ag_8, thus, planar structures are no more the ground state, and a structural transition has occurred to noncrystalline (fivefold) configurations, in agreement with previous literature:[37,40] silver clusters behave not too differently from alkali clusters,[37] which have 3D structures for $N \geq 6$.[90]

For the structures adsorbed on the surface in the ground-state (structure e1), the metal cluster is adsorbed on the defect with the same structure as the ground state that characterizes the gas phase: in particular, one of the two atoms of the dimer perpendicular to the equatorial plane is bound to the defect, whereas the other one is adsorbed on one oxygen ion on a nearest-neighbor to the vacancy on the surface. In this configuration, only two atoms interact directly with the surface, and this fact determines the lower value of the adhesion energy with respect to neighboring sizes. In the configuration e2, the metal cluster is instead adsorbed with the same structure of the configuration b of the gas phase: thanks to a compensation between a reduced metallic energy and an increased adhesion, this configuration is nearly degenerate with the ground state.

In the structures e3 and e4, the cluster is adsorbed with the same structure as in the configuration c of the gas phase, that is, the crystalline motif. In structure e3, the metal cluster is remarkably distorted due to the formation of a (distorted) square facet through which the cluster adheres to the defect and to three oxygen ions of the surface next to the vacancy, as in the case of configuration d5 of Ag_6. This structure can also be seen as a tetrahedron of ten atoms lacking two basal atoms with the (111) epitaxy distorted to a quasi-(100) epitaxy, because of the tendency to a pseudomorphic growth on the defected surface. The structure e4 is less distorted with respect to the gas-phase structure, but, due to a loss of both metallic and adhesion energy, is the highest in energy among those considered (it lies about 0.3 eV higher than the ground state).

Configuration e5 can be seen either as a distortion of configuration a of the gas phase or as an alternative fcc crystalline structure, in which two metal atoms cover the central octahedral core by adsorbing on two vicinal facets belonging to different square pyramids. In this structure, both the metallic bond and the adhesion energy are strengthened and the configuration is thus competitive with the ground state, having a total binding energy similar to that of configurations e2 and e3.

Finally, in structure e6 the metal cluster is adsorbed in a planar configuration with three metal atoms interacting with the vacancy and two nearest-neighbor oxygen atoms. With respect to the other configurations considered, in this case the adhesion energy is enhanced, but the substantial destabilization due to the weak metallic energy makes this structure higher than the ground state by about 0.5 eV.

To conclude, we note that also Ag_8 exhibits a remarkable fluxionality: four of the configurations we have described (e1, e2, e3, e5) possess very similar values of the total binding energy, although they belong to completely different structural motifs. This confirms the ability of the DF-BH approach to explore different funnels of the adsorbed cluster potential energy surface.

Ag_{10} cluster: The results concerning Ag_{10} are reported in Table 1 and the corresponding structures are displayed in Figure 6. In the same figure, the lowest energy configurations characterizing Ag_{10} in the gas phase are also displayed.

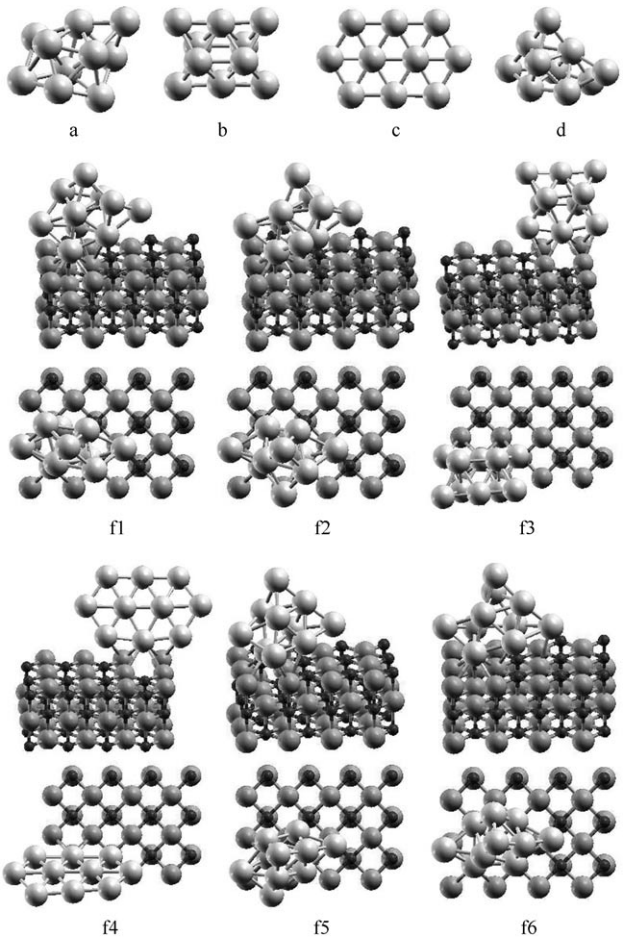

Figure 6. Schematic representation of the lowest energy structures of Ag_{10} both in the gas phase (a–d) and on the F_s-defective MgO(100) surface (f1–f6).

In the gas phase, as for Ag_8, the ground state still belongs to a noncrystalline fivefold motif: in structure a, with a cohesive energy of 15.65 eV, nine atoms constitute a fragment of the 13-atom icosahedron, while the tenth atom is external, growing on one of the (111) facets. Structure b, instead, with a cohesive energy of 15.30 eV, is a crystalline motif in which four atoms are grown symmetrically on the central octahedron core. Structure c, the cohesive energy of which is 15.53 eV, is a planar motif, portion of an fcc (111) layer. The energy difference of this planar structure with respect to the ground state is only 0.12 eV, which is not surprising because ten is a magic number for 2D circular jellium models (also due to the twofold angular degeneracy in the plane).[89] Finally, structure d, isoenergetic with structure c, can be described as a distorted fcc structure. These results are in keeping with previous literature.[37,38,40]

The ground state of Ag_{10} on the F_s-defective MgO(100) surface is given by configuration f6. Similar to configuration e3 of Ag_8, in this structure the metal cluster can be seen as a distorted tetrahedron adsorbed on the defect through one basal corner, in which the (111) epitaxy has converted to a quasi-(100) epitaxy to match the pattern of the oxygen ions of the surface; moreover, the corner of the tetrahedron more distant from the defect has moved in order to improve the adhesion to the surface. Configuration f5 is similar to f6, with the difference that the distorted metal tetrahedron is adsorbed on the vacancy through the central atom of a basal edge, and not through one basal corner: since the edge atom has a higher metal coordination, it has a weaker interaction with the defect and the adhesion energy is consequently lower with respect to the f6 ground state. The metallic energy is instead almost the same as that of the ground state and the total binding energy is lower (in absolute value) than the ground state by about 0.3 eV. Also the structure f3 belongs to the crystalline structural motif and is analogous to the configuration e4 of Ag_8. This configuration exhibits a loss of both metallic energy and adhesion to the surface and the total binding energy is lower than that of the ground state by about 1 eV.

Configuration f4 corresponds to the planar structure of the metal cluster in the gas phase: this configuration is destabilized by about 0.5 eV with respect to the ground state because of its poor adhesion to the surface.

Finally, in configurations f1 and f2 the metal cluster has the same noncrystalline structure characterizing configuration a of the gas phase. In spite of the increased metallic energy in these configurations, we have a decreased adhesion to the surface and, globally, this structural family is higher by 0.1–0.2 eV with respect to the ground state.

The main conclusion is thus that the ground-state structure of Ag_{10} adsorbed on the defected surface does not correspond to the gas-phase ground-state structure: in passing from Ag_8 to Ag_{10}, a structural transition from noncrystalline motifs, based on the pentagonal bipyramid, to distorted crystalline structures occurs. The reason of this is that the double frustration lengthens the interatomic distances between the atom adhered to the defect and its nearest-neighbors adhered to the nearby O and Mg sites; this effect disfavors noncrystalline fivefold symmetric structures, in which these distances are already strained because of the frustration inherent in decahedral or icosahedral clusters.[91] Despite the fluxionality inherent in such small clusters, this switch of preference towards crystalline structures can help explain why experimentally[31] only truncated octahedra are observed in MBE (molecular beam epitaxy) deposition experiments of Ag clusters on the MgO(100) surface, even at very small (height $\approx$1 nm, lateral width $\approx$1–2 nm) sizes, despite the fact that fivefold symmetric structures are the ground state for Ag clusters in the gas phase in this size range.[92] Even though larger clusters can be on the whole less affected by the presence of the neighboring defect, a kinetic trapping into fcc configurations might occur.

Is the cluster Ag_8 magic? It is interesting to observe that $N=8$ corresponds to an electronic magic number of the spherical jellium model.[93,94] We thus could expect a particular stability associated to this size, at least in the gas phase. Figure 7 shows the behavior of the excess energy for Ag_N clusters in the size range $N=4$–10 both in the gas phase and when adsorbed on the F_s-defective surface. The excess energy is defined in Equation (1), in which $E_b(N)$ is the metallic binding energy of the clusters in the gas phase, or the total binding energy (metallic energy plus adhesion energy) for the adsorbed clusters and ε_{coh} is the bulk fcc cohesive energy of the metal calculated within the DF/PWscf approach: 2.50 eV.

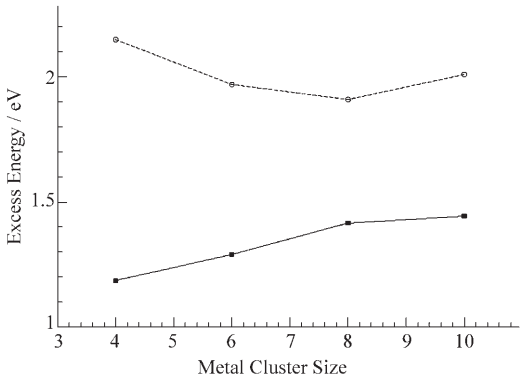

Figure 7. Excess energy as a function of cluster size for gas-phase structures (upper line with circles), and adsorbed structures (lower line with squares).

$$E_{exc}(N) = \frac{E_b(N) - N\varepsilon_{coh}}{N^{2/3}} \quad (1)$$

From Figure 7, we see that in the gas phase the cluster Ag_8 does not present an exceptional stability (somewhat at variance with the predictions of the jellium model), being only modestly favored with respect to sizes six and ten, even though a minimum in the excess energy is found at this size.

Table 2. Binding energies on the F_s [$E_{bnd}(F_s)$] and regular [E_{bnd}(reg)] surface and energy differences [$\Delta E(N \rightarrow i)$] related to the fragmentation process of an N-atom cluster into two smaller units, one (containing i atoms) still anchored to the defect and the other one (the complement of i to N) adsorbed on the regular surface. All energy values in eV.

N	$E_{bnd}(Fs)$	E_{bnd}(reg)	ΔE ($N \rightarrow 1$) Ag_1/F_s	ΔE ($N \rightarrow 2$) Ag_2/F_s	ΔE ($N \rightarrow 3$) Ag_3/F_s	ΔE ($N \rightarrow 4$) Ag_4/F_s	ΔE ($N \rightarrow 6$) Ag_6/F_s	ΔE ($N \rightarrow 8$) Ag_8/F_s
1	1.64	0.42	–	–	–	–	–	–
2	3.51	2.39	1.45	–	–	–	–	–
3	4.80	3.51	0.77	0.87	–	–	–	–
4	7.01	5.56	1.86	1.11	1.79	–	–	–
6	10.74	–	–	1.67	2.43	1.34	–	–
8	14.31	–	–	–	–	1.74	1.18	–
10	18.29	–	–	–	–	–	1.99	1.59

This is due to the fact that the valence 5s orbital of the silver atom is too expanded to fit the Ag–Ag interatomic distances, and the energy stabilization associated with the jellium shell closure is frustrated by a destructive interference of the electronic wavelength.[95] When the cluster is adsorbed on the defect, the situation is further worsened by the weak adhesion of this cluster with respect to the neighboring sizes. In order not to distort excessively with respect to the gas-phase structure, Ag_8 in fact adsorbs with only two atoms directly interacting with the surface. The final result is that the excess energy for the adsorbed clusters in this size range is an increasing function of the cluster size.

Cluster fragmentation: In analogy with previous work,[49,50,77,96] we have considered the energetics of processes corresponding to the fragmentation of the metal cluster into two pieces: the former still adsorbed on the defect, the latter adsorbed on the regular MgO(100) terrace. These processes can be important to understand the detrapping mechanism from this defect, and the process of Ostwald ripening of small clusters by bigger ones observed in MBE experiments at sufficiently high temperatures.[31] In Table 2 the energy differences corresponding to several fragmentation processes on the regular surface are reported. It is interesting to note that the lowest energy fragmentation process consists in the detachment of an Ag_2 dimer from a larger metal aggregate. This is due to the peculiar stability of Ag_2 on the regular surface. The energy associated with this process grows in an approximately monotonous way with the cluster size from 0.77 eV (the value for Ag_3 fragmentation) to 1.6 eV (the value for Ag_{10} fragmentation). With the exception of the smaller nuclearities, these processes are thus expected to be active at temperatures higher than room temperature.[31]

Conclusions

The structure of Ag_N clusters (N=1–4, 6, 8, 10) both in the gas phase and grown on the F_s-defective MgO(100) surface has been investigated by means of a density functional basin-hopping (DF-BH) approach.[36] In analogy with what already observed in the case of Au_N clusters on the F_s defect,[77] it is found that the presence of the defect implies a double frustration and a cylindrical invariance of the metal–surface interaction, causing small Ag clusters growing around the F_s defect to be highly fluxional.

For the gas-phase clusters, in agreement with the literature on the subject,[37,40] it is found that a structural transition occurs at $N=8$, such that the ground-states of Ag_N clusters are planar for $N=6$, and compact for $N=8$ and 10 with a predominance of noncrystalline, fivefold symmetric structures. The interaction with the F_s defect substantially modifies this scenario: 1) the crossover between planar and fivefold symmetric compact structures already occurs at $N=6$; 2) a further transition from fivefold symmetric to crystalline structures is found at $N=10$. The latter transition is rationalized by considering the additional strain that noncrystalline structures undergo, because of the double frustration effect due to the defect. Despite the fluxionality inherent in such small clusters, this tendency towards crystalline structures (possibly combined with kinetic trapping) could help explain why experimentally[31] only truncated octahedra are observed in MBE experiments of deposition of Ag clusters on the MgO(100) surface, even at very small (height $\approx$1 nm, lateral width $\approx$1–2 nm) sizes, despite the fact that fivefold symmetric structures are the ground state for Ag clusters in the gas phase in this size range.[92]

Moreover, Ag_8, which corresponds to a magic number of the spherical jellium model, is found to be slightly favored with respect to neighboring sizes in the gas phase, but not when adsorbed on the defected surface.

Fragmentation processes have also been investigated, finding that the lowest energy pathway corresponds to the detachment of a dimer, and that this process can be active for Ag_3 already at room temperature, or at higher temperatures for larger clusters.

Acknowledgements

G.B. and A.F. acknowledge financial support from the Italian CNR for the program "(Supra-) Self-Assemblies of Transition Metal Nanoclusters" within the framework of the ESF EUROCORES SONS, and from the European Community Sixth Framework Project for the STREP Project "Growth and Supra-Organization of Transition and Noble Metal Nanoclusters" (contract no. NMP-CT-2004-001594). E.A. was in part supported by Office of Basic Energy Sciences, U.S. Department of Energy under

Contract No. DE-AC05-00OR22725 with UT-Battelle, LLC. Calculations were performed at Cineca within an agreement with Italian CNR-INFM.

[1] H. J. Freund, *Surf. Sci.* **2002**, *500*, 271.
[2] C. R. Henry, *Surf. Sci. Rep.* **1998**, *31*, 235.
[3] G. J. Hutchings, M. Haruta, *Appl. Catal. A* **2005**, *291*, 2.
[4] C. T. Campbell, *Surf. Sci. Rep.* **1997**, *27*, 1
[5] N. Remediakis, N. Lopez, J. K. Norskov, *Appl. Catal. A* **2005**, *291*, 13.
[6] M. S. Chen, D. W. Goodman, *Science* **2004**, *306*, 252.
[7] H. Häkkinen, S. Abbet, A. Sanchez, U. Heiz, U. Landman, *Angew. Chem.* **2003**, *115*, 1335; *Angew. Chem. Int. Ed.* **2003**, *42*, 1297.
[8] A. L. de Oliveira, A. Wolf, F. Schüth, *Catal. Lett.* **2001**, *73*, 157.
[9] R. Wang, J. Hao, X. Guo, X. Wang, X. Liu, *Studies Surf. Sci. Catal.* **2004**, *154*, 2632.
[10] D. C. Lim, I. Lopez-Salido, Y. D. Kim, *Surf. Sci.* **2005**, *598*, 96.
[11] S. A. Nepijiko, D. N. Ievlev, W. Schulze, *Eur. Phys. J. D* **2003**, *24*, 115.
[12] G. Celep, E. Cottancin, J. Lermé, M. Pellarin, L. Arnaud, J. R. Huntzinger, J. L. Vialle, M. Broyer, B. Palpant, O. Boisron, P. Mélinon, *Phys. Rev. B* **2004**, *70*, 165409.
[13] J. Zheng, R. M. Dickson, *J. Am. Chem. Soc.* **2002**, *124*, 13982.
[14] M. L. Brongersma, *Nat. Mater.* **2003**, *2*, 296.
[15] I. Y. Yudanov, G. Pacchioni, K. Neyman, N. Rösch, *J. Phys. Chem. B* **1997**, *101*, 2786.
[16] A. V. Matveev, K. Neyman, I. Yudanov, N. Rösch, *Surf. Sci.* **1999**, *426*, 123.
[17] N. Lopez, F. Illas, N. Rösch, G. Pacchioni, *J. Chem. Phys.* **1999**, *110*, 4873.
[18] G. Barcaro, A. Fortunelli, *J. Chem. Theory Comput.* **2005**, *1*, 972.
[19] O. Robach, G. Renaud, A. Barbier, *Surf. Sci.* **1998**, *401*, 227.
[20] Y. C. Lee, P. Tong, P. A. Montano, *Surf. Sci.* **1987**, *181*, 559.
[21] F. Heifets, Y. F. Zhukovskii, E. A. Kotomin, M. Causà, *Chem. Phys. Lett.* **1998**, *283*, 395.
[22] J. Goniakowski, *Phys. Rev. B* **1998**, *58*, 1189.
[23] A. Sanchez, S. Abbet, U. Heiz, W. D. Schneider, H. Häkkinen, R. N. Barnett, U. Landman, *J. Phys. Chem. A* **1999**, *103*, 9573.
[24] L. Giordano, G. Pacchioni, *Surf. Sci.* **2005**, *575*, 197.
[25] L. M. Molina, B. Hammer, *J. Chem. Phys.* **2005**, *123*, 161104.
[26] H. Moseler, H. Häkkinen, U. Landman, *Phys. Rev. Lett.* **2002**, *89*, 176103.
[27] A. Bogicevic, D. R. Jennison, *Surf. Sci.* **1999**, *437*, L741.
[28] C. Sousa, F. Illas, *J. Chem. Phys.* **2001**, *115*, 1435.
[29] P. Mori-Sanchez, J. M. Recio, B. Silvi, C. Sousa, A. Martin Pendas, V. Luana, F. Illas, *Phys. Rev. B* **2002**, *66*, 075103.
[30] S. Wendt, Y. D. Kim, D. W. Goodman, *Prog. Surf. Sci.* **2003**, *74*, 141.
[31] C. Revenant, G. Renaud, R. Lazzari, J. Jupille, *Nucl. Instrum. Methods Phys. Res. Sect. B* **2006**, *246*, 112.
[32] G. Barcaro, A. Fortunelli, *New J. Phys.* **2007**, *9*, 22.
[33] A. Ouahab, C. Mottet, J. Goniakowski, *Phys. Rev. B* **2005**, *72*, 035421.
[34] H. M. Benia, N. Nilius, H. J. Freund, *Surf. Sci.* **2006**, *600*, L128.
[35] G. Haas, A. Menck, H. Brune, J. V. Barth, J. A. Venables, K. Kern, *Phys. Rev. B* **2000**, *61*, 11105.
[36] E. Aprà, R. Ferrando, A. Fortunelli, *Phys. Rev. B* **2006**, *73*, 205414.
[37] E. M. Fernández, J. M. Soler, I. L. Garzón, L. C. Balbás, *Phys. Rev. B* **2004**, *70*, 165403.
[38] V. Bonacic-Koutecky, L. Cespiva, P. Fantucci, J. Koutecky, *J. Chem. Phys.* **1993**, *98*, 7981.
[39] V. Bonacic-Koutecky, L. Cespiva, P. Fantucci, J. Pittner, J. Koutecky, *J. Chem. Phys.* **1994**, *100*, 490.
[40] R. Fournier, *J. Chem. Phys.* **2001**, *115*, 2165.
[41] L. N. Kantorovich, J. M. Holender, M. J. Gillan, *Surf. Sci.* **1995**, *343*, 221.
[42] G. Pacchioni, P. Pescarmona, *Surf. Sci.* **1998**, *412/413*, 657.
[43] J. Carrasco, N. Lopez, F. Illas, *Phys. Rev. Lett.* **2004**, *93*, 225502.
[44] J. Carrasco, N. Lopez, F. Illas, H. J. Freund, *J. Chem. Phys.* **2006**, *125* 074711.
[45] Z. Yan, S. Chinta, A. A. Mohamed, J. P. Fackler, D. W. Goodman, *J. Am. Chem. Soc.* **2005**, *127*, 1604.
[46] G. Pacchioni, *ChemPhysChem* **2003**, *4*, 1041.
[47] J. Kramer, W. Ernst, C. Tegenkamp, H. Pfnur, *Surf. Sci.* **2002**, *517*, 87.
[48] M. Sterrer, M. Yulikov, E. Fischbach, M. Heyde, H. P. Rust, G. Pacchioni, T. Risse, H. J. Freund, *Angew. Chem.* **2006**, *118*, 2692; *Angew. Chem. Int. Ed.* **2006** *45*, 2630.
[49] C. Inntam, L. V. Moskaleva, K. M. Neymanm V. A. Nasluzov, N. Rosch, *Appl. Phys. A* **2006**, *82*, 181.
[50] K. M. Neyman, C. Inntam, L. V. Moskaleva, N. Rösch, *Chem. Eur. J.* **2006**, *12*, 277.
[51] K. M. Neyman, C. Inntam, A. V. Matveev, V. A. Nasluzov, N. Rosch, *J. Am. Chem. Soc.* **2005**, *127*, 11652.
[52] L. M. Molina, B. Hammer, *Appl. Catal. A* **2005**, *291*, 21.
[53] R. Coquet, G. J. Hutchings, S. H. Taylor, D. J. Willock, *J. Mater. Chem.* **2006**, *16*, 1978.
[54] Y. F. Zhukovskii, E. A. Kotomin, P. W. M. Jacobs, A. M. Stoneham, *Phys. Rev. Lett.* **2000**, *84*, 1256.
[55] A. Bogicevic, D. R. Jennison, *Surf. Sci.* **2002**, *515*, L481.
[56] A. Del Vitto, G. Pacchioni, F. Delbecq, P. Sautet, *J. Phys. Chem. B* **2005**, *109*, 8040.
[57] A. S. Wörz, K. Judai, S. Abbet, J. M. Antonietti, U. Heiz, A. Del Vitto, L. Giordano, G. Pacchioni, *Chem. Phys. Lett.* **2004**, *399*, 266.
[58] M. Arenz, U. Landman, U. Heiz, *ChemPhysChem* **2006**, *7*, 1871.
[59] B. Yoon, H. Häkkinen, U. Landman, A. S. Wörz, J. M. Antonietti, S. Abbet, K. Judai, U. Heiz, *Science* **2005**, *307*, 403.
[60] M. Walter, H. Häkkinen, *Phys. Rev. B* **2005**, *72*, 205440.
[61] M. Sterrer, E. Fischbach, T. Risse, H. J. Freund, *Phys. Rev. Lett.* **2005**, *94*, 186101.
[62] M. Sterrer, M. Heyde, M. Novicki, N. Nilius, T. Risse, H. P. Rust. G. Pacchioni, H. J. Freund, *J. Phys. Chem. B* **2006**, *110*, 46.
[63] M. Chiesa, M. C. Paganini, E. Giamello, D. M. Murphy, C. Di Valentin, G. Pacchioni, *Acc. Chem. Res.* **2006**, *39*, 861.
[64] Y. D. Kim, J. Stultz, T. Wei, D. W. Goodman, *J. Phys. Chem. B* **2002**, *106*, 6827.
[65] A. Kolmakov, J. Stultz, D. W. Goodman, *J. Chem. Phys.* **2000**, *113*, 7564.
[66] Z. Li, H. A. Scheraga, *Proc. Natl. Acad. Sci. USA* **1987**, *84*, 6611.
[67] D. J. Wales, J. P. K. Doye, *J. Phys. Chem. A* **1997**, *101*, 5111.
[68] D. J. Wales, H. A. Scheraga, *Science* **1999**, *285*, 1368.
[69] Through movements of the metal atoms of up to ± 1 Å in each cartesian direction.
[70] K. Jug, T. Bredow, *J. Comput. Chem.* **2004**, *25*, 1551.
[71] G. Pacchioni, A. M. Ferrari, A. M. Marquez, F. Illas, *J. Comput. Chem.* **1997**, *18*, 617.
[72] P. J. Hay, W. R. Wadt, *J. Chem. Phys.* **1985**, *82*, 270; P. J. Hay, W. R. Wadt, *J. Chem. Phys.* **1985**, *82*, 299.
[73] I. V. Iudanov, V. A. Nasluzov, K. M. Neyman, N. Rösch, *Int. J. Quantum Chem.* **1997**, *65*, 975.
[74] Z. Yang, R. Wu, Q. Zhang, D. W. Goodman, *Phys. Rev. B* **2002**, *65* 155407.
[75] V. A. Nasluzov, V. V. Rivanenkov, A. B. Gordienko, K. M. Neyman, U. Birkenheuer, N. Rösch, *J. Chem. Phys.* **2001**, *115*, 8157.
[76] K. M. Neyman, C. Inntam, V. A. Nasluzov, R. Kosarev, N. Rösch, *Appl. Phys. A* **2004**, *78*, 823.
[77] G. Barcaro, A. Fortunelli, *J. Phys. Chem. B* **2006**, *110*, 21021.
[78] R. A. Kendall, E. Aprà, D. E. Bernholdt, E. J. Bylaska, M. Dupuis, G. I. Fann, R. J. Harrison, J. Ju, J. A. Nichols, J. Nieplocha, T. P. Straatsma, T. L. Windus, A. T. Wong, *Comput. Phys. Commun.* **2000**, *128*, 260.
[79] J. P. Perdew, J. A. Chevary, S. H. Vosko, K. A. Jackson, M. R. Pederson, D. J. Singh, C. Fiolhais, *Phys. Rev. B* **1992**, *46*, 6671.
[80] A. Schaefer, C. Huber, R. Ahlrichs, *J. Chem. Phys.* **1994**, *100*, 5289.
[81] D. Andrae, U. Haeussermann, M. Dolg, H. Stoll, H. Preuss, *Theor. Chim. Acta* **1990**, *77*, 123.
[82] The double-ζ basis is formed by two s functions with exponents $\alpha_s = 0.32$ and $\alpha_s = 0.12$, and a p function, contraction of two gaussians with exponents of $\alpha_p = 0.18$ and $\alpha_p = 0.05$; for the triple-ζ basis we

added an s function with $\alpha_s = 0.025$, we split the two contracted p functions and added a d function with exponent of $\alpha_d = 0.08$.
[83] F. Weigend, M. Haser, H. Patzel, R. Ahlrichs, *Chem. Phys. Lett.* **1998**, *294*, 143.
[84] C. Elsässer, M. Fähnle, C. T. Chan, K. M. Ho, *Phys. Rev. B* **1994**, *49*, 13975; R. W. Warren, B. I. Dunlap, *Chem. Phys. Lett.* **1996**, *262*, 384.
[85] S. Baroni, A. Del Corso, S. de Gironcoli, P. Giannozzi: http://www.pwscf.org.
[86] J. P. Perdew, K. Burke, M. Ernzerhof, *Phys. Rev. Lett.* **1996**, *77*, 3865.
[87] Y. F. Zhukovskii, E. A. Kotomin, D. Fucks, S. Dorfman, *Superlattices Microstruct.* **2004**, *36*, 63.
[88] C. W. Bauschlicher, S. R. Langhoff, H. Partridge, *J. Chem. Phys.* **1990**, *93*, 8133.
[89] E. Janssens, H. Tanaka, S. Neukermans, R. E. Silverans, P. Lievens, *New J. Phys.* **2003**, *5*, 46.
[90] I. A. Solov'yov, A. V. Solov'yov, W. Greiner, *Phys. Rev. A* **2002**, *65*, 053203.
[91] F. Baletto, R. Ferrando, *Rev. Mod. Phys.* **2005**, *77*, 371.
[92] F. Baletto, C. Mottet, R. Ferrando, *Phys. Rev. Lett.* **2000**, *84*, 5544.
[93] W. Ekardt, *Phys. Rev. B* **1984**, *29*, 1558.
[94] D. E. Beck, *Solid State Commun.* **1984**, *49*, 381.
[95] R. Ferrando, A. Fortunelli, G. Rossi, *Phys. Rev. B* **2005**, *72*, 085449.
[96] L. J. Xu, G. Henkelman, C. T. Campbell, H. Jonsson, *Surf. Sci.* **2006**, *600*, 1351.

Received: December 14, 2006
Published online: May 11, 2007

